Scientific paper

Studies on Morphology and Photoluminescent Properties of Tb^{3+} Doped $YbPO_4$ Nanostructures Synthesized by Different Synthetic Methods

Heena Khajuria, Manesh Kumar, Lobzang Tashi, Rajinder Singh, and Haq Nawaz Sheikh*

Department of Chemistry, University of Jammu, Jammu 180006, India

* *Corresponding author: E-mail: hnsheikh@rediffmail.com*

Received: 05-23-2019

Abstract

The morphology dependent optical properties of Tb^{3+} in $YbPO_4$ host lattice have been investigated. 10 % Terbium doped ytterbium phosphate ($YbPO_4$:Tb^{3+}) nanostructures (NSs) were synthesized by five different synthetic methods i.e. sonochemical method, hydrothermal method, solvothermal method, sacrificial template method and coprecipitation method. Structural facets and optical properties of fabricated nanoparticles were studied in detail by powder X-ray diffraction (PXRD), Fourier transform infrared spectrum (FTIR), scanning electron microscopy (SEM), transmission electron microscopy (TEM), energy dispersive X-ray spectra (EDS), and photoluminescence (PL) techniques. We have investigated the impact of synthetic procedures employed on the morphology and uniformity of synthesized NSs and consequently on the optical properties of the NSs. The intense green emission from the nanophosphor shows that phosphor can be used in IR-sensors, LEDs and as solar spectrum converters.

Keywords: Sonochemical synthesis; hydrothermal synthesis; solvothermal synthesis; sacrificial template synthesis; co-precipitation synthesis; luminescence

1. Introduction

Phosphate compounds are suitable host matrices for lanthanide ions to fabricate luminescent substances. Among $LnPO_4$, ytterbium phosphate ($YbPO_4$), is well-known useful host lattice (materials) for lanthanide ions for the synthesis of phosphors .[1–3] The optical properties of lanthanide based phosphors mostly depend on their shape, size, surface chemistry, uniformity and dimensionality. In general luminescent materials with small particle size have lower luminescence quantum efficiency and shorter fluorescence lifetime than larger particle size materials or their bulk counterparts.[4,5] This is owing to low crystallinity and large number of surface defects associated with them. Reducing the size of particle to nano dimensions cause increase in the surface-to-volume ratio of the material which leads to dominance of surface effects.[6–10] In addition to this, the presence of ligands/capping agents and surface-adsorbed ions/molecules (H_2O, CO_2) also lead to luminescence quenching. Molecules in proximity to surface of nanoparticles can diminish the intensity, since the vibrational states of chemical bonds like O-H, C-H or N-H match the phonon states of the host material resulting in non-radiative relaxation of the excited lanthanide ions.[11,12] These structural aspects in turn can be controlled by the synthesis methods and reaction conditions.[13–17] The photoluminescent nanomaterials can be fabricated by various techniques *viz.*, hydrothermal, solvothermal, sonochemical assisted thermal decomposition, and co-precipitation etc. Hydrothermal and solvothermal methods endow some convenient advantages over the conventional methods, such as potential to control over the crystal growth, its simplicity and relatively low temperature for reaction.[18-20] These methods permit exceptional control over morphology, particle size and crystallinity of material. Among these techniques, sonochemical method is the best method to synthesize nanostructures because it is green synthesis method carried out at room temperature.[21] It is based on acoustic cavitation resulting from the continuous formation, growth and implosive collapse of bubbles in a liquid. It has become one of the useful, green, simple and fast methods for the synthesis as well as doping of nanostructures. Apart from these, the sacrificial template-directed chemical synthetic method based on the Kirkendal effect

has been established to be an effective approach to obtain the desired hollow inorganic materials.[22,23] In this method, the shell of desired product forms around the surface of the sacrificial template and takes the shape of the template. Thus, various physicochemical changes evolved in the synthesis of nonmaterial under different synthetic conditions influence the phase, morphology and properties of nanostructures.

In the present work, 10% Terbium doped ytterbium phosphate ($YbPO_4:Tb^{3+}$) nanostructures were synthesized by five different synthetic methods such as hydrothermal method, solvothermal method, sacrificial template method, sonochemical method and co-precipitation method to study their effect on morphology and luminescent properties of as prepared nanomaterials. Tb^{3+} is chosen as dopant for doping $YbPO_4$ host matrices. Yb^{3+} ions act as sensitizer ion for Tb^{3+} ions which shows green emission. [24–26] $YbPO_4:Tb^{3+}$ nanostructures were examined by powder X-ray diffraction (PXRD), Fourier transform infrared spectrum (FTIR), scanning electron microscopy (SEM), transmission electron microscopy (TEM), energy dispersive X-ray spectra (EDS), and photoluminescence (PL) techniques. The effect of synthesis method on the uniformity, structure and the optical properties of the $YbPO_4:Tb^{3+}$ nanostructures were studied in detail. Nanostructures of different morphology have been obtained through different synthesis routes. The intense green emission from the nanophosphor shows that phosphor can be used in IR-sensors, LEDs and as solar spectrum converters. The novelty aspect and the significance of the present work with respect to the existing literature reports on related nanostructures lies in the tunning of pholuminesence emission intensity by varying the morphology and grain size of synthesized phosphors via five different synthetic methods.

2. Experimental

2. 1. Materials

Ytterbium (III) nitrate pentahydrate $Yb(NO_3)_3 \cdot 5H_2O$ (99.9 %), terbium(III) nitrate hydrate $Tb(NO_3)_3 \cdot H_2O$ (99.9 %) and ammonium dihydrogen phosphate were purchased from Alfa Aesar (Massachusetts, United States) and used as received without further purification. Urea was purchased from Himedia (Mumbai, India) and sodium hydroxide from Sigma Aldrich (United States). Deionized water was used throughout.

2. 2. Synthesis of $YbPO_4:Tb^{3+}$ Nanostructures

2. 2. a Sonochemical Method

In a typical synthesis, 20 mL aqueous solution of 0.9 mmol $Yb(NO_3)_3 \cdot H_2O$ and 0.1 mmol $Tb(NO_3)_3 \cdot H_2O$ was sonicated for 15 minutes. Thereafter 10 mL aqueous solution of 1 mmol $NH_4H_2PO_4$ was added dropwise to the above mentioned mixture. The pH of solution is maintained at 3 by adding ammonia solution. The mixture was then sonicated for additional 1 h. After that, the precipitates were collected and washed with deionised water and ethanol and then dried at 70 °C for 12 hrs.

2. 2. b Hydrothermal method

In a typical synthesis, 0.9 mmol (0.344 g) of $Yb(NO_3)_3 \cdot 5H_2O$ was added to 10 mL aqueous solution of 1 mmol (0.1921 g) citric acid. The reaction mixture was stirred for 10 minutes and after that an aqueous solution of 0.5 mmol (0.057 g) $NH_4H_2PO_4$ was added dropwise. After further vigorous stirring for 30 minutes more, as obtained mixture was transferred into a autoclave, sealed and maintained at 180 °C for 18 hrs. Once the autoclave cooled to room temperature naturally, the precipitates were collected, centrifuged and washed with deionised water and ethanol three times and then dried at 70 °C for 12 hrs. in air.[27]

2. 2. c Solvothermal Method

In a typical synthesis, 0.9 mmol (0.323 g) of $Yb(NO_3)_3 \cdot 5H_2O$ and 0.1 mmol (0.034 g) $Tb(NO_3)_3 \cdot H_2O$ were added to mixture of 5 mL oleic acid and 5 mL ethylene glycol. The reaction mixture was vigorously stirred for 10 minutes. After that solution of 0.5 mmol (0.057 g) $NH_4H_2PO_4$ in ethylene glycol was added dropwise to the above mentioned reaction mixture. After further stirring for 30 minutes, the mixture so obtained was transferred into autoclave, sealed and heated at 180 °C for 18 hrs. The autoclave was cool to room temperature naturally; the product was centrifuged, washed with deionised water, followed by ethanol then dried at 70 °C for 12 hrs. in air.

2. 2. d Coprecipitation Method

20 mL aqueous solution of 0.9 mmol (0.323 g) of $Yb(NO_3)_3 \cdot 5H_2O$ and 0.1 mmol (0.034 g) $Tb(NO_3)_3 \cdot H_2O$ and 20 mL aqueous solution of $NH_4H_2PO_4$ was stirred for 15 min. Two solutions were mixed together and stirred for another 10 minutes. After that solution of NaOH was added to reaction mixture of $Yb(NO_3)_3 \cdot 5H_2O$, $Tb(NO_3)_3 \cdot H_2O$ and $NH_4H_2PO_4$. The reaction mixture was vigorously stirred at 80 °C for 30 minutes. The as prepared sample was collected, centrifuged, washed with deionised water and ethanol three times and then dried at 70 °C for 12 h in air.[28]

2. 2. e Sacrificial Template Method

Synthesis of $Yb(OH)CO_3$: 10 mol% Tb^{3+} template: The $Yb(OH)CO_3:Tb^{3+}$ precursor was prepared by urea-based homogeneous precipitation process. In a typical synthesis, 0.9 mmol (0.323 g) $Yb(NO_3)_3 \cdot 5H_2O$ and 0.1 mmol (0.034 g) $Tb(NO_3)_3 \cdot H_2O$ were dissolved in 50 mL deionized water. Then, 2.0 g of urea was added into the as prepared lan-

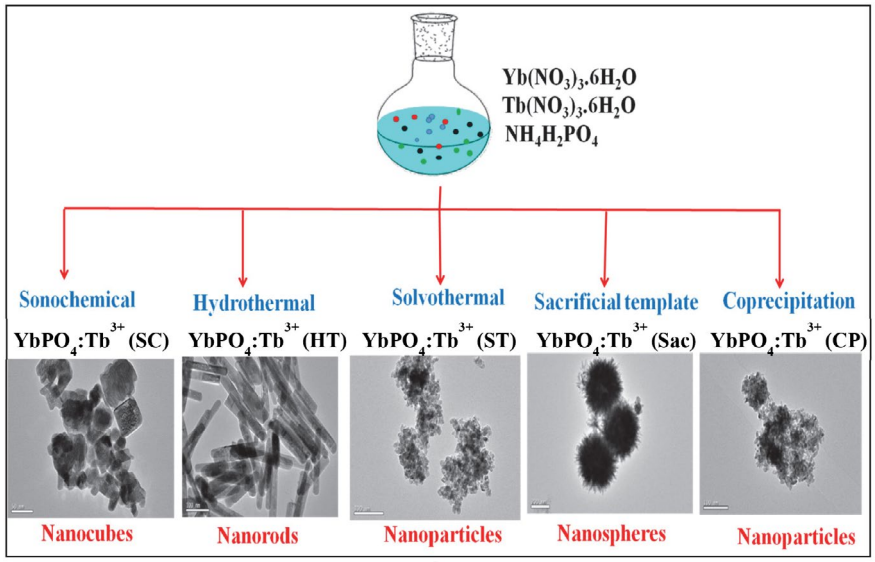

Figure 1. Overview of obtained $YbPO_4:Tb^{3+}$ nanostructures

thanide aqueous solution with continues stirring. The solution was stirred vigorously for 2 h at room temperature and heated to 90 °C for another 2 h in an oil bath in order to get the milky-white suspension. The precipitated $Yb(OH)CO_3:Tb^{3+}$ were filtered and then washed with ethanol and deionised water three times.

Synthesis of $YbPO_4$: 10 mol% Tb^{3+} : In a typical synthesis, the as-prepared sample of $Yb(OH)CO_3:Tb^{3+}$ rods acting as template was dispersed into 15 mL deionized water by ultrasonic treatment for 30 min, labelled as solution A. A separate solution B was prepared by dissolving 1 mmol (0.115 g) $NH_4H_2PO_4$ in 15 mL deionised water and mixed with solution A with vigorous agitation. Finally, 30 mL of the resulting reaction mixture was transferred into Teflon lined stainless steel autoclave, seal and heated at 180 °C for 18 hrs. The autoclave was cool down to room temperature naturally. The products were collected, centrifuged and washed with DI water and ethanol three times and dried at 60 °C for 24 hrs in air.[29]

The samples prepared by sonochemical method, hydrothermal method, solvothermal method, sacrificial template method and coprecipitation method are designated as $YbPO_4:Tb^{3+}$ (SC), $YbPO_4:Tb^{3+}$ (HT), $YbPO_4:Tb^{3+}$ (ST), $YbPO_4:Tb^{3+}$ (Sac), $YbPO_4:Tb^{3+}$ (CP) respectively as shown in Fig. 1.

2. 3. Characterization

The crystalline structure of the powder samples was assessed by X-ray diffraction using a Panalytical Xpert Pro diffractometer with Cu-Kα radiation at 45 kV and 40 mA, and 2θ ranging from 10° to 70°. The infrared spectra of NRs were measured on a Shimadzu Prestige-21 Fourier Transform spectrometer over the range of wave number 4000 – 400 cm^{-1}, and standard KBr pellet technique was employed. The morphology of the samples was inspected using a field emission scanning electron microscope (FE-SEM) and transmission electron microscope (TEM). TEM images were taken using a Hitachi (H-7500) transmission electron microscope at an accelerating voltage of 100 kV. To obtain the TEM images, ethanolic solution of the sample is first subjected to sonication to form a very fine suspension. 10 µL of this suspension is then carefully poured onto a carbon copper grid using a micropipette and dried under an electric light. The dried samples are then loaded into the TEM machine. SEM was performed using Nova Nano SEM-450 field emission scanning electron microscope at an accelerating voltage of 5.0 kV. For getting SEM images, the well dried samples are fixed on a metal grid with adhesive, dehydrated and then observed in the microscope. Steady state excitation and emission spectra of the samples were recorded on a Cary Eclipse spectrophotometer equipped with a Xenon lamp as the excitation source. The analysis of optical property of prepared samples was conducted in the powder form, as the lanthanide phosphates are insoluble in most of the solvents. All of the measurements were performed at room temperature.

Particle size determination

Each SEM image has a measurement scale at the bottom left corner for size measurements. Using *Image J software*, particle size of each clearly visible nanoparticle in the image was measured. After size of all of the nanoparticles was measured, a histogram was created in order to show the size distribution of the nanoparticles in each sample.

3. Results and Discussion

3. 1. PXRD Measurements

The crystalline nature and phase purity of the as prepared nanocomposites were explored by PXRD study. Fig.

2 depicts powder X-ray diffraction patterns of the undoped $YbPO_4$, $YbPO_4$:Tb^{3+} (SC), $YbPO_4$:Tb^{3+} (HT), $YbPO_4$:Tb^{3+} (ST), $YbPO_4$:Tb^{3+} (Sac) and $YbPO_4$:Tb^{3+} (CP) nanostructures. The PXRD patterns of all prepared phases are in good agreement with the tetragonal phase of $YbPO_4$ (JCPDS card no. 45-0530) space group ($I4_1/amd$).[30, 31] No other phase impurity was detected by PXRD analysis, demonstrating the phase purity of as prepared nanostructure. The result indicates that the doping of Tb^{3+} ions in the $YbPO_4$ nanocrystals has little influence on its crystal structure due to the similar ionic radius of Tb^{3+} = (0.104 nm) and Yb^{3+} = (0.098 nm). The broadened peaks in PXRD patterns suggest the nano range of as prepared nanomaterials. The broadening of PXRD peaks can be correlated with the particle size measured from SEM images using *Image J software*. The particle size of $YbPO_4$:Tb^{3+} (SC), $YbPO_4$:Tb^{3+} (HT), $YbPO_4$:Tb^{3+} (ST), $YbPO_4$:Tb^{3+} (Sac), and $YbPO_4$:Tb^{3+} (CP) nanostructures is found to be ~ 170 nm, ~ 600 × 80 nm, ~ 70 nm, ~ 300-400 nm, ~100 nm respectively from SEM images. The observed particle size of nanostructures is in accordance to the broadening of PXRD peaks.

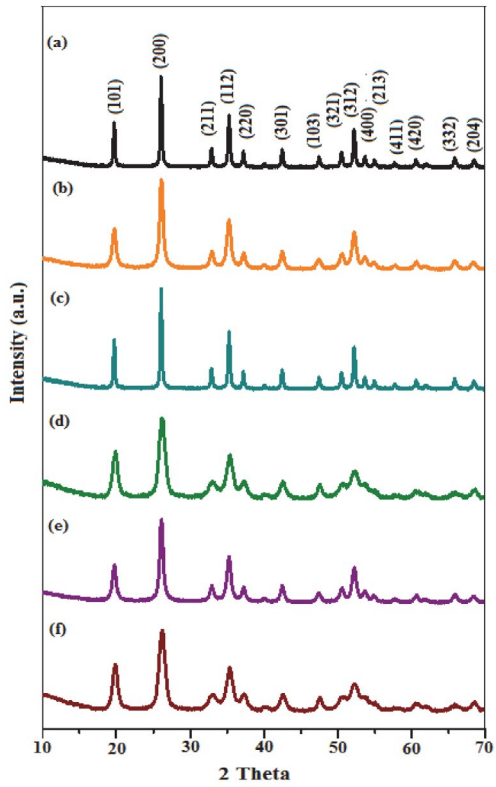

Figure 2. PXRD patterns of (a) undoped $YbPO_4$ (b) $YbPO_4$:Tb^{3+} (SC) (c) $YbPO_4$:Tb^{3+} (HT) (d) $YbPO_4$:Tb^{3+} (ST) (e) $YbPO_4$:Tb^{3+} (Sac) (f) $YbPO_4$:Tb^{3+} (CP)

3. 2. FTIR Spectra

The presence of chelating agent and chemical composition on the surface of the nanomaterials have been examined by FT-IR spectra. Fig. 3 shows the FT-IR spectra of undoped $YbPO_4$, $YbPO_4$:Tb^{3+} (SC), $YbPO_4$:Tb^{3+} (HT), $YbPO_4$:Tb^{3+} (ST), $YbPO_4$:Tb^{3+} (Sac) and $YbPO_4$:Tb^{3+} (CP) nanostructures. The bands near 1100 cm^{-1} are assigned the stretching modes of the PO_4^{3-} groups of as prepared samples. The splitting of the band indicated the presence of low symmetry crystal phase. The two characteristics bending vibrational modes of the PO_4^{3-} group are at 650 and 520 cm^{-1}.[32, 33] It can be noted that when $YbPO_4$ host is doped Tb^{3+} ions the infra red band around 1100 cm^{-1} slightly shifted to higher wave number because of stronger interaction between Tb^{3+} and PO_4^{3-} as compare to Yb^{3+} and PO_4^{3-} units.[34] The presence of hydroxyl groups and water molecules on surface of synthesized nanomaterials can be ascertained by infrared bands in the range of 3200-3600 cm^{-1} (stretching vibrations) and 1625 cm^{-1} (bend-

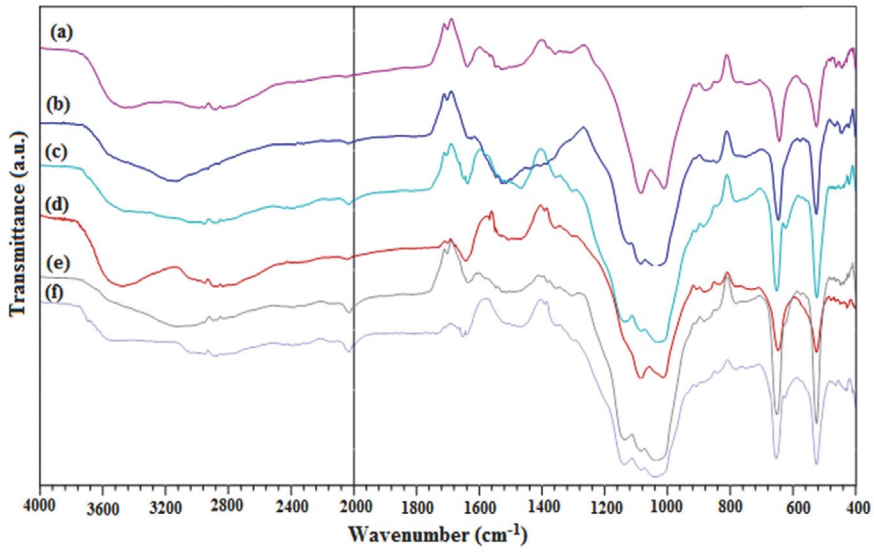

Figure 3. FTIR spectra of (a) undoped $YbPO_4$ (b) $YbPO_4$:Tb^{3+} (SC) (c) $YbPO_4$:Tb^{3+} (HT) (d) $YbPO_4$:Tb^{3+} (ST) (e) $YbPO_4$:Tb^{3+} (Sac) (f) $YbPO_4$:Tb^{3+} (CP)

ing). The characteristic IR bands (υ_{as}1680 and υ_s 1384 cm^{-1}) of ligands (citric acid and oleic acid) are not appeared clearly in FTIR spectra of $YbPO_4$:Tb^{3+} (HT) and $YbPO_4$:Tb^{3+} (ST) due to their overlapping with other peaks.

3. 3. SEM and TEM Studies

The structured and morphological facets of the as synthesized nanostructuires were probed by the scanning electron microscopy (SEM) and transmission electron mi-

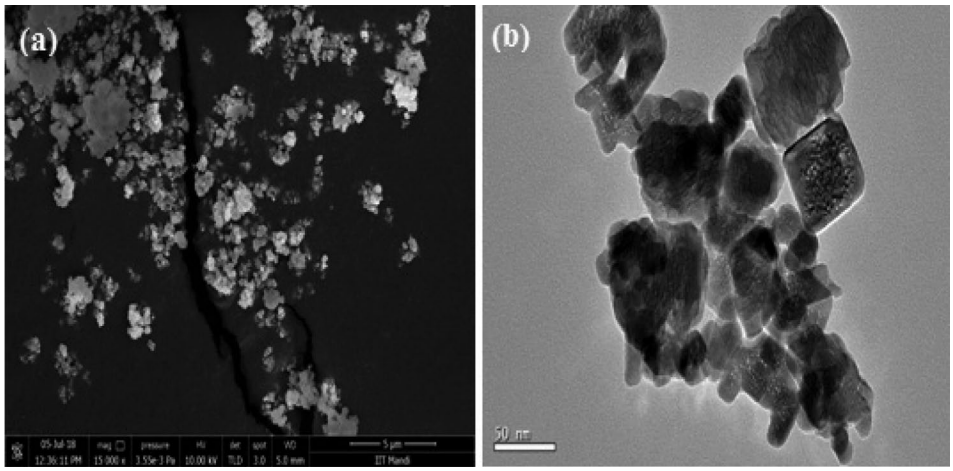

Figure 4. (a) SEM and (b) TEM images of $YbPO_4$:Tb^{3+} (SC)

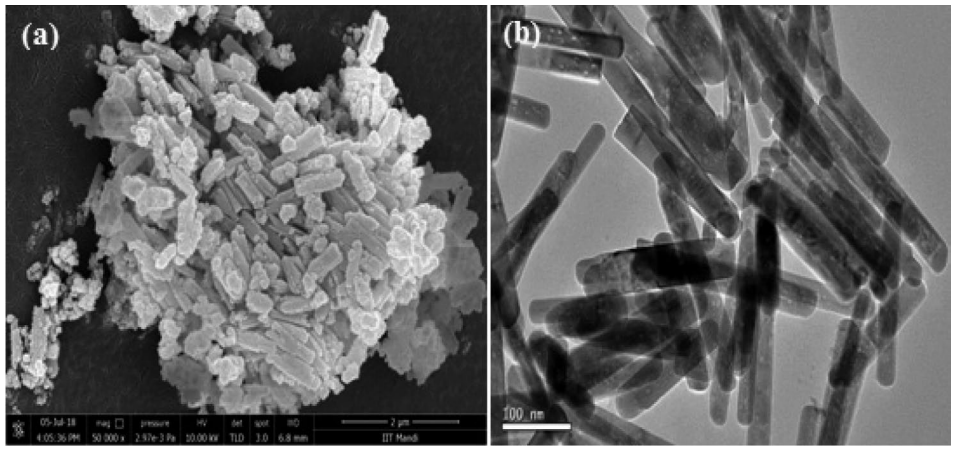

Figure 5. (a) SEM and (b) TEM images of $YbPO_4$:Tb^{3+} (HT)

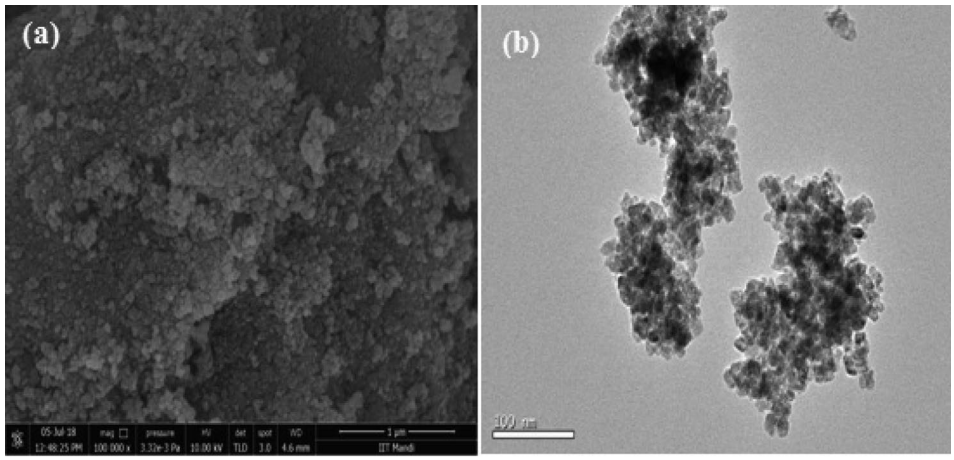

Figure 6. (a) SEM and (b) TEM images of $YbPO_4$:Tb^{3+} (ST)

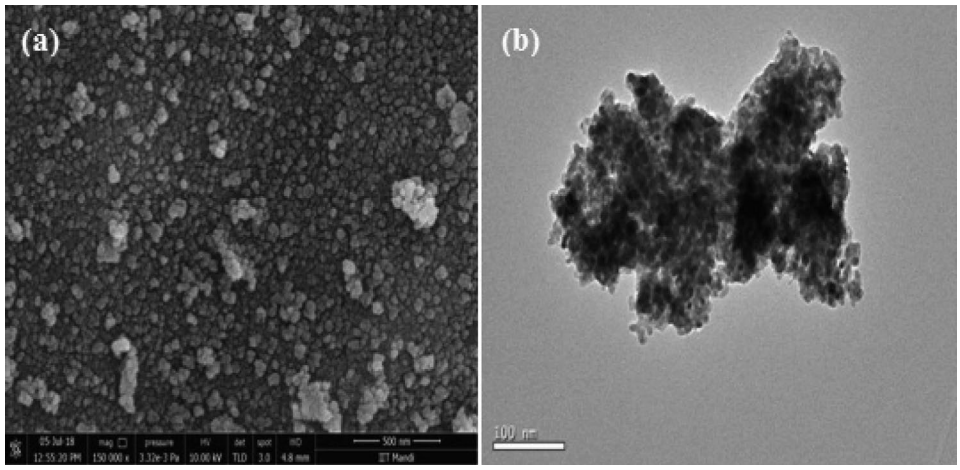

Figure 7. (a) SEM and (b) TEM images of $Yb(OH)CO_3$:Tb^{3+} precursor

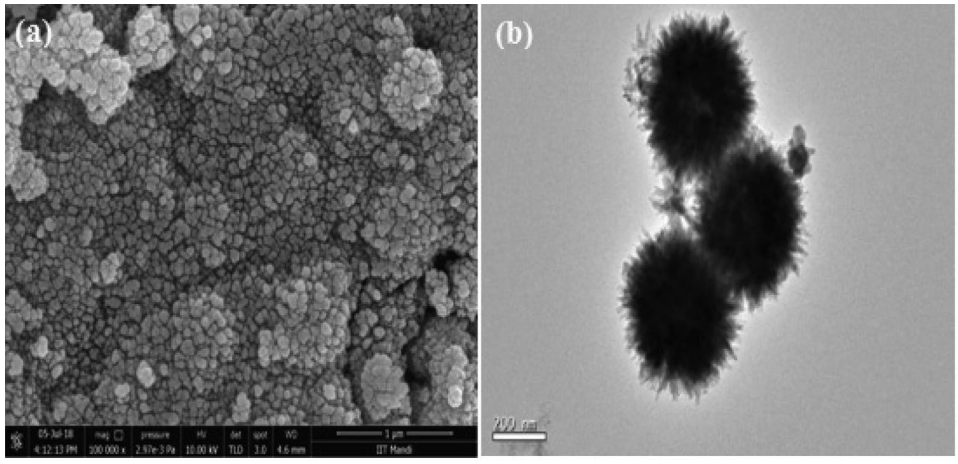

Figure 8. (a) SEM and (b) TEM images of $YbPO_4$:Tb^{3+} (Sac)

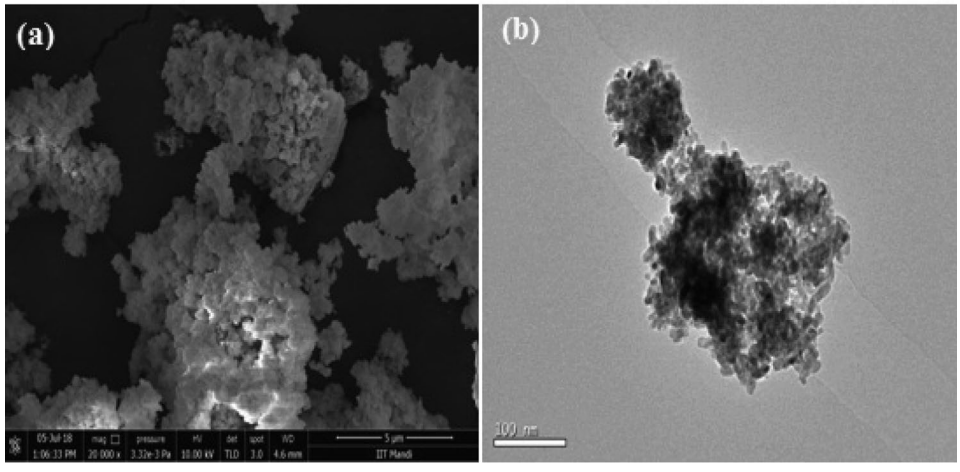

Figure 9. (a) SEM and (b) TEM images of $YbPO_4$:Tb^{3+} (CP)

croscopy (TEM) analysis. The scanning electron and transmission electron micrographs of terbium doped ytterbium phosphate nanocomposite as synthesized via different synthetic procedures are shown in Figs. 4–9. SEM images of $YbPO_4$:Tb^{3+} (SC) dispose the square shaped flakes like morphology of particle size ~ 170 nm. The nanorods like morphology of $YbPO_4$:Tb^{3+} of size 600 × 80 nm was obtained via hydrothermal method (Fig 5). The $YbPO_4$:Tb^{3+} samples synthesized by solvothermal and co-precipitation method show the nanoparticles like mor-

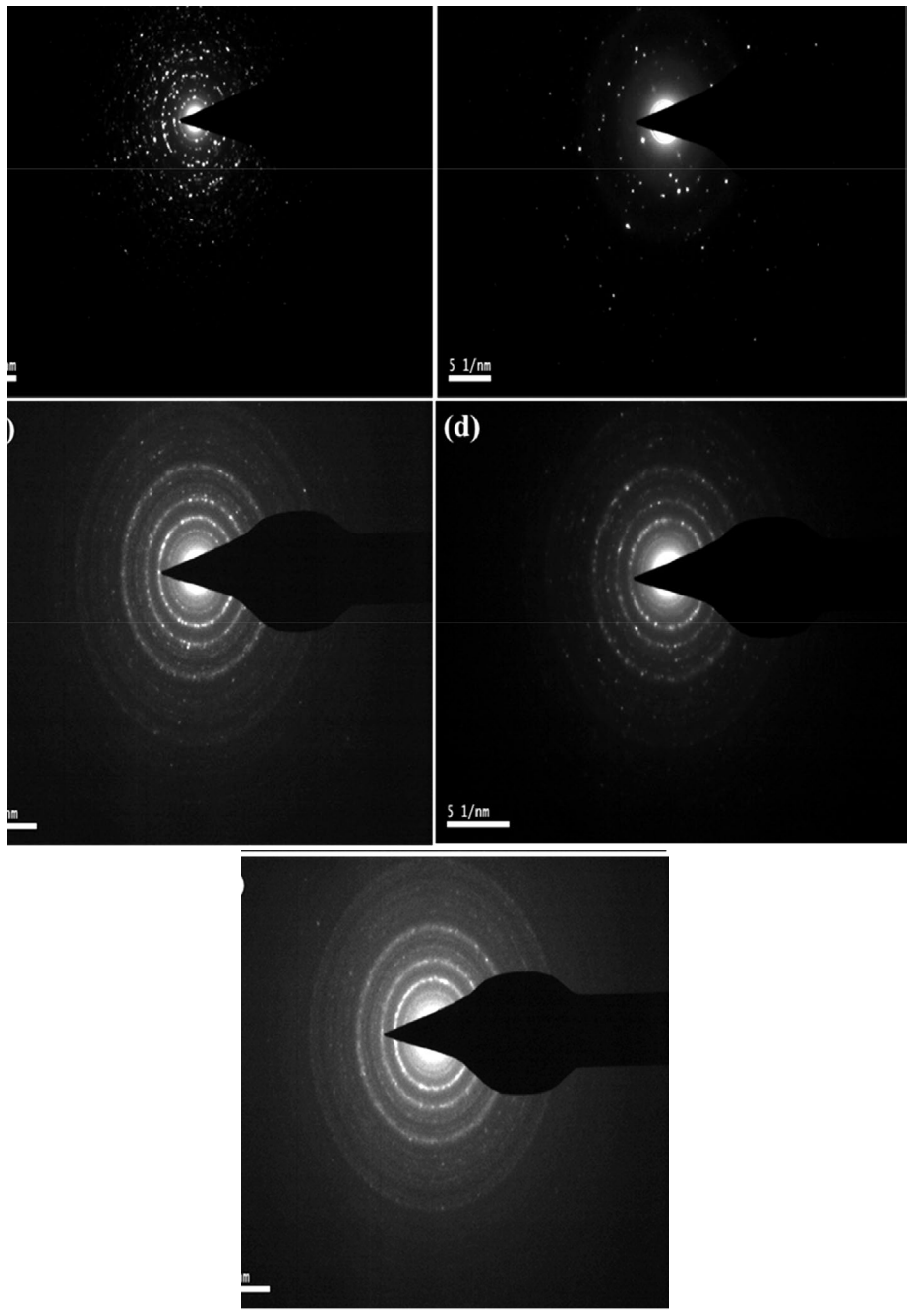

Figure 10. SAED pattern of (a) $YbPO_4$:Tb^{3+} (SC) (b) $YbPO_4$:Tb^{3+} (HT) (c) $YbPO_4$:Tb^{3+} (ST) (d) $YbPO_4$:Tb^{3+} (Sac) (e) $YbPO_4$:Tb^{3+} (CP)

phology with particle size of 70 and 100 nm respectively. The oleic acid and ethylene glycol may play role in the fabrication of nanoparticles. The overall mechanism of their action is such that their molecules embrace the nanocrystals and control their excess growth. Thus, in these syntheses, small sized particles are obtained. Fig. 7 shows Yb(OH)CO_3:Tb^{3+} precursor SEM and TEM micrographs. It shows the spherical morphology of precursor. After its treatment with phosphate source spherical $YbPO_4$:Tb^{3+} nanostructures are formed with diameter 300-400 nm and display rather rough morphological features as compare to the precursor nanostructures. Thus, nanostructures of different morphology are obtained when synthesis is carried out by different synthetic methods. TEM images also agree well with the SEM results. The selected area electron diffraction (SAED) patterns of as synthesized nanomaterial were shown in Fig. 10. The presence of bright spots in SAED patterns of $YbPO_4$:Tb^{3+} (SC) and $YbPO_4$:Tb^{3+} (HT) indicate their monocrystalline nature (Fig. 10 a, b). However, SAED patterns of $YbPO_4$:Tb^{3+} (ST), $YbPO_4$:Tb^{3+} (Sac) and $YbPO_4$:Tb^{3+} (CP) shows diffuse rings indicating their polycrystalline nature.

3. 4. EDS Analysis

Energy dispersive X-ray spectra were recorded to investigate the presence of dopant (Tb^{3+}) and it concentration in the doped $YbPO_4$ nanoparticles represented in Fig. 11. The EDS results suggest that the nanocrystal fabricated $YbPO_4$:Tb^{3+} nanostructures are makeup of Yb, Tb, P and O. Table 1 represent the weight percent (Wt. %) and atomic percent (At. %) data for synthesized $YbPO_4$:Tb^{3+} phases. There is a slight variation in weight and atomic % of constituents is found, as synthesized by different synthetic routes.

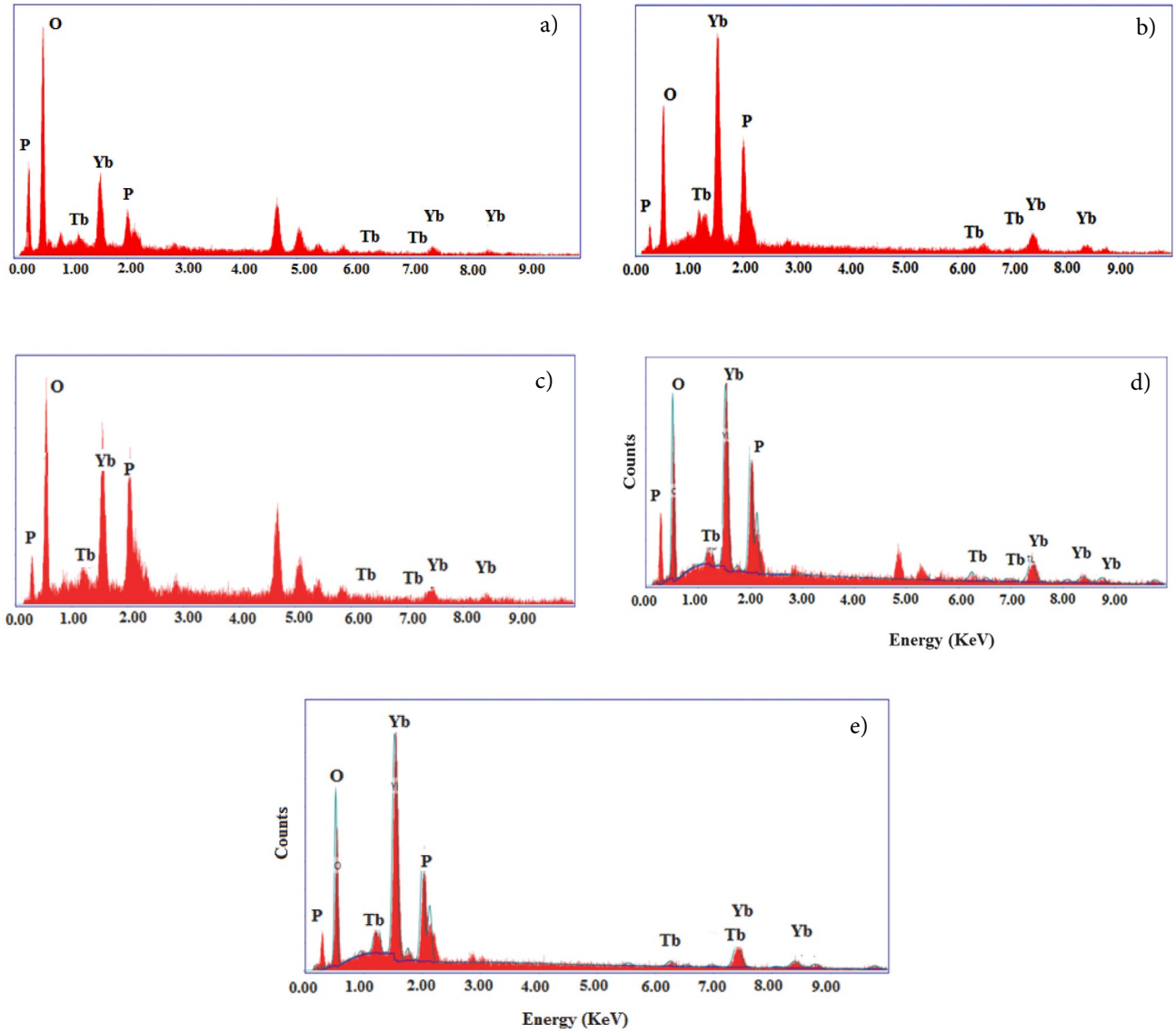

Figure 11. EDS spectra of (a) $YbPO_4$:Tb^{3+} (SC) (b) $YbPO_4$:Tb^{3+} (HT) (c) $YbPO_4$:Tb^{3+} (ST) (d) $YbPO_4$:Tb^{3+} (Sac) (e) $YbPO_4$:Tb^{3+} (CP)

Table 1. Atomic and Weight % of elements present in $YbPO_4$:Tb^{3+} nanostructures

Elements	$YbPO_4$:Tb^{3+} (SC)		$YbPO_4$:Tb^{3+} (HT)		$YbPO_4$:Tb^{3+} (HT)		$YbPO_4$:Tb^{3+} (HT) (HT)		$YbPO_4$:Tb^{3+} (CP)	
	Wt. %	At. %	Wt.%	At. %	Wt. %	At. %	Wt. %	At. %	Wt. %	At. %
Ytterbium	30.93	4.82	51.48	12.51	34.22	5.34	58.16	16.46	56.39	14.72
Terbium	9.27	1.57	8.48	2.24	0.42	0.07	8.78	2.71	7.53	2.14
Phosphorus	8.91	7.77	15.71	21.32	19.30	16.83	13.73	21.70	13.70	19.98
Oxygen	50.88	85.83	24.33	63.93	46.05	77.75	19.33	59.14	22.37	63.16

3. 5. Photoluminescence

The excitation and emission photoluminescence spectra of $YbPO_4$:Tb^{3+} nanostructures are shown in Fig. 12 and Fig. 13 respectively. We have selectively monitored excitation of Tb^{3+} doped $YbPO_4$ nanostructures at 543 nm ($^5D_4 \rightarrow {}^7F_5$ transition). The prominent peaks in the range of 200–280 nm may be attributed to the transitions of $4f^8 \rightarrow 4f^7 5d^1$ of Tb^{3+}.[35] The other weak excitation bands ranging from 300–400 nm can be assigned to the *f–f* transition of Tb^{3+}. These bands are significant for emission spectra exhibited by UV-Chips.[36] The highest intensity peak at 370 nm is due to $^7F_6 \rightarrow {}^5G_6$ transition of Tb^{3+}. The excitation spectra of $YbPO_4$:Tb^{3+} nanostructures imply that the phosphor can convert ultraviolet wavelength to visible wavelength on emission. Thus the conversion of ultraviolet light into visible light indicates that the fabricated $YbPO_4$:Tb^{3+} can act as ultraviolet light absorber in solar cells to show effective conversion efficiency. In the emission spectrum of $YbPO_4$:Tb^{3+} four prominent peaks near 490, 543, 584 and 621 nm are observed when selectively excited at 394 nm. These emission peaks are assigned to the transitions $^5D_4 \rightarrow {}^7F_6$ (490 nm), $^5D_4 \rightarrow {}^7F_5$ (543 nm), $^5D_4 \rightarrow {}^7F_4$ (584 nm) and $^5D_4 \rightarrow {}^7F_3$ (621 nm).[37] The $^5D_4 - {}^7F_5$ transition is stronger comparing with other transitions and is responsible for green light emission. From the PL spectra, the variation in the emission intensity is observed for $LaPO_4$:Tb^{3+} prepared in different conditions. It is worth noting that $YbPO_4$:Tb^{3+} (Sac) exhibit highest and $YbPO_4$:Tb^{3+} (ST) possess least intense emission.

The difference in photoluminescence intensity can be interpreted from surface area, and particle size aspects of phosphor, as PL intensity is highly affected by these parameters.[38-41] It is well established fact that the surface area of nanoparticles increases with a decrease in crystallite size. In general, larger the surface area, higher will be the defects into the crystal of a phosphor.[42, 43] It is seen that defects into phosphor crystal have serious impact on photoluminescence emission of materials. These defects lead to non-radioactive decay of electrons and holes recombination. The number of electron/hole recombinations via radiative pathways must be increased in order to generate intense emission from the material. The efficiency of radiative decay can be enhanced by defects minimizations which in turn can controlled by the degree of crystallinity and surface area. The efficiency of radiative decay can be improved by increasing crystallinity and decreasing surface area. From the SAED and XRD patterns shown in Fig. 2 and Fig. 10, it is clear that the all the prepared samples are highly crystalline. However, they differ in their particle size and morphology. Herein, the particle size for $YbPO_4$:Tb^{3+} in the descending order are $YbPO_4$:Tb^{3+} (Sac) > $YbPO_4$:Tb^{3+} (HT) > $YbPO_4$:Tb^{3+} (SC) > $YbPO_4$:Tb^{3+} (CP) > $YbPO_4$:Tb^{3+} (ST) which is consistent with the luminescence intensity. Highest PL intensity is observed from $YbPO_4$:Tb^{3+} (Sac) which may be due to its larger particle size, spherical morphology and lower surface area. $YbPO_4$:Tb^{3+} prepared by hydrothermal method possesses nanorods like morphology. The phosphors with nanorod morphology presented directional growth and lower surface area resulting in the enhanced emission intensity. The particle sizes of the samples prepared by sonochemical and coprecipitation methods are lower than that of $YbPO_4$:Tb^{3+} (Sac) and $YbPO_4$:Tb^{3+} (HT) and PL intensity is also less intense than that of $YbPO_4$:Tb^{3+} (Sac) and $YbPO_4$:Tb^{3+} (HT) indicating correlation of particle size and PL intensity. The particle size of the $YbPO_4$:Tb^{3+} (ST) is lowest and thus, surface area will be highest. Therefore, it can be interpreted that a number of holes and electron in the excited state may be expected to return to the ground state through non-radiative decay processes. Thus, it possesses lowest PL intensity. Moreover, another reason for their lowest PL intensity may be the presence of surface adsorbed solvent molecules which quenches the radiative transition.

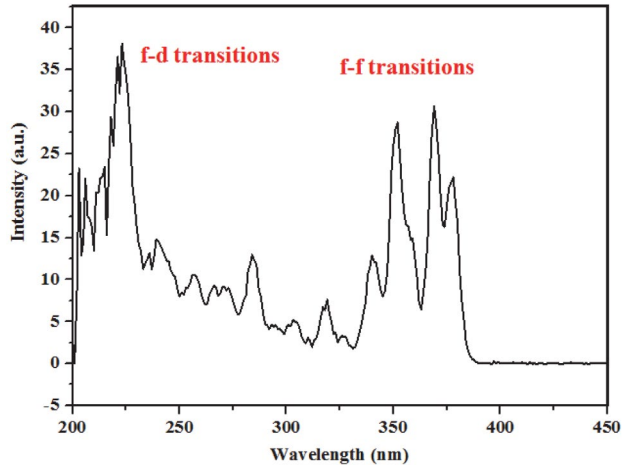

Figure 12. Excitation spectra of $YbPO_4$:Tb^{3+} nanostructures

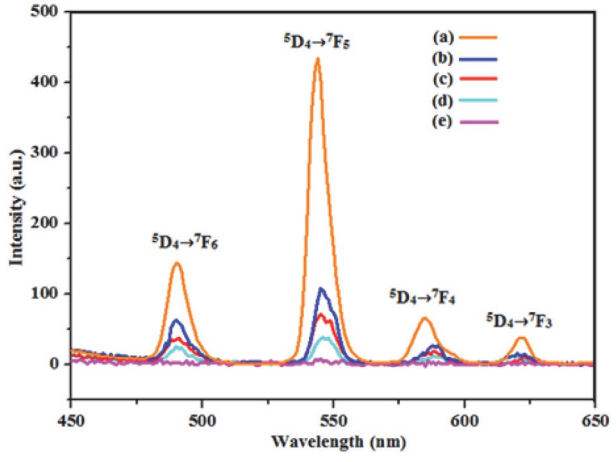

Figure 13. Emission spectra of (a) $YbPO_4$:Tb^{3+} (Sac) (b) $YbPO_4$:Tb^{3+} (HT) (c) $YbPO_4$:Tb^{3+} (SC) (d) $YbPO_4$:Tb^{3+} (CP) (e) $YbPO_4$:Tb^{3+} (ST)

4. Conclusions

$YbPO_4:Tb^{3+}$ nanostructures have been synthesized using five different synthetic methods i.e. sonochemical, hydrothermal, solvothermal, coprecipitation and sacrificial template assisted method. Tetragonal phase of $YbPO_4:Tb^{3+}$ nanostructures have been confirmed by PXRD study. SEM and TEM studies show the nanorods, nanosphere and nanoparticle like morphology of $YbPO_4:Tb^{3+}$ prepared by different methods. Variation in intensity of Tb^{3+} emission peaks is found for $YbPO_4:Tb^{3+}$ nanostructures synthesized by different methods. The difference in photoluminescence intensity can be interpreted in terms of surface area and crystallite size aspects of phosphor. Smaller is the particle size, larger would be the surface area. This results in larger number of defects in the crystal lattice which in turn has negative impact on photoluminescence efficiency. Highly intense Tb^{3+} emission peaks are observed for $YbPO_4:Tb^{3+}$ spheres having diameter 300-400 nm prepared by sacrificial template method and least intense that for $YbPO_4:Tb^{3+}$ nanoparticles obtained by solvothermal method with crystallite size of 70 nm. This shows the dependence of photoluminescence on morphology and particle size. The intense green emission from the $YbPO_4:Tb^{3+}$ phosphor indicates that phosphor can be used in LEDs.

Acknowledgements

We would like to acknowledge Advanced Material Research Centre (AMRC), IIT Mandi, SMVDU Katra for PL studies and Sophisticated Analytical Instrumentation Facility (SAIF), Panjab University for their technical support.

5. References

1. Z. Wenyan, N. Yaru, H. Wenjuan, L. Chunhua, X. Zhongzi, *J. Rare Earths* **2010**, *28*, 299–302. **DOI**:10.1016/S1002-0721(10)60337-7
2. Z. Xu, P. Ma, C. Li, Z. Hou, X. Zhai, S. Huang, J. Lin, *Biomaterials* **2011**, *32,* 4161–4173. **DOI**:10.1016/j.biomaterials.2011.02.026
3. S. Lee, K. Teshima, S. Mori, M. Endo, S. Oishi, Cryst. Growth Des. **2010**, *10,* 1693–1698. **DOI**:10.1021/cg9012729
4. F. Wang, J. Wang, X. Liu, *Angew. Chem. Int Ed.* **2010,** *49,* 7456–7460. **DOI**:10.1002/anie.201003959
5. N. K. Sahu, R. S. Ningthoujam, D. J. Bahadur, *Appl. Phys.* **2012,** *112,* 014306 (1–12). **DOI**:10.1063/1.4731644
6. J. C. Boyer, M. P. Manseau, J. I. Murray, F. C. J. M. van Veggel, *Langmuir* **2010,** *26,* 1157–1164. **DOI**:10.1021/la902260j
7. A. Yin, Y. Zhang, L. Sun, C. Yan, *Nanoscale* **2010,** *2,* 953–959. **DOI**:10.1039/b9nr00397e
8. A. Huignard, V. Buissette, A.-C. Franville, T. Gacoin, J.-P. Boilot, *J. Phys. Chem. B* **2003,** *107*, 6754–6759. **DOI**:10.1021/jp0342226
9. X. Bai, H. Song, G. Pan, Z. Liu, S. Lu, W. Di, X. Ren, Y. Lei, Q. Dai, L. Fan, *Appl. Phys. Lett.* **2006,** *88*, 143104 (1–3). **DOI**:10.1063/1.2187518
10. R. S. Loitongbam, N. S. Singh, W. R. Singh, R. S. Ningthoujam, *J. Lumin.* **2013**, *134,* 14–23. **DOI**:10.1016/j.jlumin.2012.09.026
11. Y. Wang, L.P. Tu, J. W. Zhao, Y. J. Sun, X. G. Kong, H. Zhang, *J. Phys. Chem. C* **2009**, *113*, 7164–7169. **DOI**:10.1021/jp9003399
12. H. Schafer, P. Ptacek, K. Kompe, M. Haase, *Chem. Mater.* **2007**, *19*, 1396–1400. **DOI**:10.1021/cm062385b
13. Y. Yang, *Mater.* Sci. Eng. B 2013, 178, 807–810. **DOI**:10.1016/j.mseb.2013.03.017
14. T. Grzyb, A. Gruszeczka, R. J. Wiglusz, S. Lis, *J. Mater. Chem. C* **2013**, *1*, 5410–5418. **DOI**:10.1039/c3tc31100g
15. M. Yang, H. You, Y. Huang, G. Jia, Y. Song, N. Guo, K. Liu, Y. Zheng, H. Zhang, *CrystEngComm.* **2010**, *12*, 2865–2870. **DOI**:10.1039/b921258b
16. S. Devi, S. Kelkar, V. Kashid, H. G. Salunke, N. M. Gupta, *RSC Adv.* **2013**, *3*, 16817–16828. **DOI**:10.1039/c3ra43477j
17. S. Kar, S. K. Panda, B. Satpati, P. V. Satyam, S. Chaudhuri, *J. Nanosci. Nanotechnol.* **2006**, *6*, 1-6. **DOI:**10.1166/jnn.2006.532
18. K. Byrappa, T. Adschiri, *Prog. Cryst. Growth & Charact.* **2007**, *53*, 117–166. **DOI**:10.1016/j.pcrysgrow.2007.04.001
19. M. Shandilya, R. Rai, J. Singh, *Adv. Appl. Ceram.* **2016**, *115*, 354–376. **DOI**:10.1080/17436753.2016.1157131
20. H. Hayashi, Y. Hakuta, *Materials* **2010**, *3*, 3794–3817. **DOI**:10.3390/ma3073794
21. H. Xu, B. W. Zeiger, K. S. Suslick, *Chem. Soc. Rev.* **2013**, *42*, 2555–2567. **DOI**:10.1039/C2CS35282F
22. G. Li, L. Li, M. Li, Y. Song, H. Zou, L. Zou, X. Xu, S. Gan, *Mater. Chem. Phys.* **2012**, *133*, 263–268. **DOI**:10.1016/j.matchemphys.2012.01.020
23. B. Yan, X. Xiao, *Nanoscale Res. Lett.* **2010**, *5*, 1962–1969. **DOI**:10.1007/s11671-010-9733-8
24. T. Grzyb, R. J. Wiglusz, A. Gruszeczka, S. Lis, *Dalton Trans.* **2014**, *43*, 17255–17264. **DOI**:10.1039/C4DT02234C
25. T. Grzyb, K. Kubasiewicz, A. Szczeszak, S. Lis, *Dalton Trans.* **2015**, *44*, 4063–4069. **DOI**:10.1039/C4DT03667K
26. K. Prorok, M. Pawlyta, W. Stręk, A. Bednarkiewicz, *Chem. Mater.* **2016**, *28,* 2295–2300. **DOI**:10.1021/acs.chemmater.6b00353
27. H. Khajuria, J. Ladol, S. Khajuria, M.S. Shah, H.N. Sheikh, *Mater. Res. Bull.* **2016**, *80*, 150–158. **DOI**:10.1016/j.materresbull.2016.03.022
28. S. Verma, K. K. Bamzai, *J. Rare Earths* **2015**, *33*, 535–544. **DOI**:10.1016/S1002-0721(14)60453-1
29. Z. Yi, W. Lu, C. Qian, T. Zeng, L. Yin, H. Wang, L. Rao, H. Liu, S. Zeng, *Biomater. Sci.* **2014,** *2,* 1404–1411. **DOI**:10.1039/C4BM00158C
30. W. Wang, D. Xu, X. Wei, K. Chen, *Int. J. Nanomedicine* **2014**, *9*, 4879–4891. **DOI**:10.2147/IJN.S62678
31. W. O. Milligan, D. F. Mullica, G. W. Beall, L. A. Boatner, Structures of $ErPO_4$, $TmPO_4$, and $YbPO_4$, *Acta Cryst C* **1983**, *39*, 23–24. **DOI**:10.1107/S0108270183003467
32. M. Ferhi, K. H. Naifer, M. Ferid, *J. Rare Earths* **2009**, *27*, 182–186. **DOI**:10.1016/S1002-0721(08)60216-1

33. G. M. Begun, G. W. Beall, L. A. Boatner, W. J. Gregor, *J. Raman Spectrosc*. **1981**, *11*, 273–278. **DOI**:10.1002/jrs.1250110411
34. K. N. Konou, M. Haris, Y. Lare, M. Baneto, K. Napo, *Pramana J. Phys*. **2016**, *87*, 1–7. **DOI**:10.1007/s10854-017-7857-7
35. M. L. Debasu, D. Ananias, J. Rocha, O. L. Malta, L. D. Carlos, *Phys. Chem. Chem. Phys.* **2013**, *15*, 15565–15571. **DOI**:10.1039/c3cp52365a
36. W. B. Bu, Z. L. Hua, L. X. Zhang, H. R. Chen, W. M. Huang, J. L. Shia, *J. Mater. Res.* **2004**, *19*, 2807–2811. **DOI**:10.1557/JMR.2004.0388
37. H. Khajuria, J. Ladol, S. Khajuria, M. S. Shah, H. N. Sheikh, *Mater. Res. Bull.* **2016**, *80*, 150–158. **DOI**:10.1016/j.materresbull.2016.03.022
38. W. Wang, W. Widiyastuti, T. Ogi, I. W. Lenggoro, K. Okuyama, *Chem. Mater.* **2007**, *19*, 1723–1730. **DOI**:10.1021/cm062887p
39. L. Bin, J. Li, G. Duan, Q. Li, Z. Liu, *J. Lumin*. **2019**, *206*, 348–358. **DOI**:10.1016/j.jlumin.2018.10.035
40. T. Han, C. Zhang, X. Cheng, L. Peng, S. Cao, *Nanosci. Nanotechnol. Lett.* **2017**, *9*, 328–332. **DOI**:10.1166/nnl.2017.2290
41. S. Prashant, K. Sharma, R. K. Dutta, A. C. Pandey, J. *Appl. Phys*. **2012**, *112* 054321(1-5). **DOI**:10.1063/1.4751335
42. A. Kar, S. Kundu, A. Patra, J. Phys. Chem. C **2011**, *115*, 118–124. **DOI**:10.1021/jp110313b
43. J. Ding, Z. Lian, Y. Li , S. Wang, Q. Yan, J. Phys. Chem. Lett. **2018,** *9*, 4221–4226. **DOI**:10.1021/acs.jpclett.8b01898

Povzetek

Preučevali smo odvisnost optičnih lastnosti od morfologije $YbPO_4$ dopiranega s Tb^{3+}. Nanodelce s terbijem dopiranega iterbijevega fosfata ($YbPO_4$:Tb^{3+}) smo pripravili s petimi različnimi sinteznimi metodami: sonokemično metodo, hidrotermalno metodo, solvotermalno metodo, z metodo kemijske pretvorbe delcev z ohranitvijo oblike in metodo koprecipitacije. Strukturne in optične lastnosti nanodelcev smo preučevali z rentgensko praškovno difrakcijo (PXRD), infrardečo spektroskopijo (FTIR), vrstično elektronsko mikroskopijo (SEM), presevno elektronsko mikroskopijo, energijsko disperzijsko spektroskopijo rentgenskih žarkov (EDS) in meritvami fotoluminiscence (PL). Preučevali smo vpliv uporabljenega sinteznega pristopa na morfologijo in homogenost nanodelcev in posledično na optične lastnosti materiala. Intenzivna emisija zelene svetlobe kaže na to, da bi lahko material uporabili za IR senzorje, LED diode in v fotovoltaiki.